



HAL
open science

Experimental study of sono-crystallisation of $\text{ZnSO}_4 \cdot 7\text{H}_2\text{O}$, and interpretation by the segregation theory

H. Harzali, Fabien Baillon, Olivier Louisnard, Fabienne Espitalier, A. Mgaidi

► **To cite this version:**

H. Harzali, Fabien Baillon, Olivier Louisnard, Fabienne Espitalier, A. Mgaidi. Experimental study of sono-crystallisation of $\text{ZnSO}_4 \cdot 7\text{H}_2\text{O}$, and interpretation by the segregation theory. *Ultrasonics Sonochemistry*, 2011, 18 (5), pp.1097-1106. 10.1016/j.ultsonch.2011.03.007 . hal-01678807

HAL Id: hal-01678807

<https://hal.science/hal-01678807>

Submitted on 5 Sep 2018

HAL is a multi-disciplinary open access archive for the deposit and dissemination of scientific research documents, whether they are published or not. The documents may come from teaching and research institutions in France or abroad, or from public or private research centers.

L'archive ouverte pluridisciplinaire **HAL**, est destinée au dépôt et à la diffusion de documents scientifiques de niveau recherche, publiés ou non, émanant des établissements d'enseignement et de recherche français ou étrangers, des laboratoires publics ou privés.

Experimental study of sono-crystallisation of $\text{ZnSO}_4 \cdot 7\text{H}_2\text{O}$, and interpretation by the segregation theory

H. Harzali ^{a,b}, F. Baillon ^a, O. Louisnard ^{a,*}, F. Espitalier ^a, A. Mgaidi ^b

^a Centre RAPSODEE, FRE CNRS 3213, Université de Toulouse, Ecole des Mines d'Albi, 81013 Albi Cedex 09, France

^b Industrial Inorganic Chemistry Laboratory, Chemistry Department, Faculty of Sciences, Tunis 1060, Tunisia

A B S T R A C T

Power ultrasound is known to enhance crystals nucleation, and nucleation times can be reduced by one up to three orders of magnitude for several organic or inorganic crystals. The precise physics involved in this phenomenon still remains unclear, and various mechanisms involving the action of inertial cavitation bubbles have been proposed. In this paper, two of these mechanisms, pressure and segregation effects, are examined. The first one concerns the variations of supersaturation induced by the high pressures appearing in the neighbourhood of a collapsing bubble, and the second one results from the modification of clusters distribution in the vicinity of bubble. Crystallisation experiments were performed on zinc sulphate heptahydrate $\text{ZnSO}_4 \cdot 7\text{H}_2\text{O}$, which has been chosen for its pressure-independent solubility, so that pressure variations have no effect on supersaturation. As observed in past studies on other species, induction times were found lower under insonification than under silent conditions at low supersaturations, which casts some doubts on a pure pressure effect. The interfacial energy between the solid and the solution was estimated from induction times obtained in silent conditions, and, using classical nucleation theory, the steady-state distribution of the clusters was calculated. Segregation theory was then applied to calculate the over-concentrations of n -sized clusters at the end of the collapse of a $4 \mu\text{m}$ bubble driven at 20 kHz by different acoustic pressures. The over-concentration of clusters close to the critical size near a collapsing bubble was found to reach more than one order of magnitude, which may favour the direct attachment process between such clusters, and enhance the global nucleation kinetics.

Keywords:

Ultrasound

Nucleation

Segregation

Induction time

Zinc sulphate heptahydrate

Acoustic cavitation

1. Introduction

Crystallisation is a process used in many industrial domains including chemical, pharmaceutical and petro-chemical industries, and usually considered in terms of nucleation and crystal growth [1]. Works on the influence of ultrasound in crystallisation processes have been published for several years [2–6]. The positive influence of ultrasound on crystallisation processes is shown by the drastic reduction of the induction time, metastable zone width, the modification of the crystals size distribution and the increase in the number of crystals at equivalent supersaturation [2].

The precise mechanism of the effect of ultrasound on nucleation is yet unclear [7,8]. Various theoretical explanations involving the action of inertial cavitation bubbles have been described in the literature:

1. *Cooling hypothesis*: the solubility of crystals generally decreases as the temperature is lowered, and when the bubble expands, the cooling of the neighbouring liquid may therefore increase supersaturation, on a short timescale [8].

2. *Pressure hypothesis*: when the bubble collapses, the neighbouring liquid suffers high pressure, up to 1 GPa. Pressure variations shift the thermodynamical equilibrium between the solute and the solid phase [9]. For species which are denser in solid form than in solute form, increasing pressure decreases solubility, so that high pressures appearing near the bubble collapse would increase supersaturation and therefore enhance nucleation. [8,6,10].

3. *Evaporation hypothesis*: solvent evaporation into the bubble may produce a depletion layer of solvent near the bubble wall, leading to an local increase of the solute concentration and therefore of supersaturation. This hypothesis has been mentioned in Ref. [11] on the basis of the results of Ref. [12], but has not been explored theoretically.

4. Finally, it has been recently proposed [13], and quantified theoretically [10], that the large acceleration of the bubble at the end of the collapse could segregate the solute and the crystal precursors from the solvent during a very short time, enhancing the global nucleation kinetics.

All these effects sound reasonable and may in fact act in a complementary fashion. The partial or total invalidation of one of these hypothesis requires additional sono-crystallisation data.

* Corresponding author.

E-mail address: louisnar@enstima.fr (O. Louisnard).

Nomenclature

Symbols

a	activity
a_{eq}	activity at equilibrium
C_0	molecular concentration of possible nucleating sites
C_S	molar concentration of the solid
C_{eq}	equilibrium molar concentration of the solution
C_n	pseudo-equilibrium concentration of (n)-cluster
c	a shape factor
D_n	diffusion coefficient of a (n)-cluster in the solution
f	frequency of ultrasound
J_S	nucleation rate
K	pre-factor for interfacial-tension calculation
k_B	Boltzmann constant
k_{nm}	kinetic constant of attachment between a (n)-cluster and a (m)-cluster
l_{mn}	kinetic constant of detachment of a (m)-cluster
M	molar mass
n	number of monomers in a cluster
n^*	number of monomers in the critical cluster
Pe	Peclet number
p	pressure
p_0	ambient pressure
R_0	ambient radius of the bubble
S	supersaturation ratio ($= \frac{a}{a_{eq}}$)
T	temperature
t	time

t_{ind}	induction time
V	volume of the solution
\bar{v}_L	specific molecular volume of solute
v_S	molecular volume of the solid
W^*	nucleation work
$W(n)$	work necessary to form a (n)-cluster
X_n	concentration of (n)-cluster for stationary nucleation
$X_{seg}(n)$	concentration of the clusters at the bubble wall
Z_n	concentration of (n)-cluster
z	Zeldovich factor

Greek symbols

β	parameter representing the difference in the densities of the two segregated species
γ	interfacial tension between solid and solution
γ_{\pm}	mean molal activity coefficient
η	dynamic viscosity
ϕ	osmotic coefficient of water
$\Delta\mu$	driving force for nucleation
ρ	density of the solution
ρ_S	density of the solid
ω	mass-fraction of dissolved solid in the solution
ω_{eq}	equilibrium mass-fraction of dissolved solid in the solution
$\Delta\omega$	absolute supersaturation

The crystal of interest must be conveniently selected in view of its pertinent physical properties involved in the above-mentioned phenomena.

Past studies have revealed that ultrasound also enhances nucleation of species which solubility increases with pressure [2,11]. This casts some doubts on the reality of the pressure effect, which mechanism is recalled in Section 2, and, as an additional confirmation, we sought a crystal which solubility is pressure-independent. Zinc sulphate heptahydrate (referred hereinafter as $ZnSO_4 \cdot 7H_2O$) was found to have this property. We performed crystallisation experiments by cooling crystallisation, with and without ultrasound. The experimental protocol and the results are presented in Section 3. In Section 4, nucleation of $ZnSO_4 \cdot 7H_2O$ is examined in the light of classical nucleation theory, and the segregation hypothesis is examined by quantifying the over-concentration of crystal precursors induced by an inertial cavitation bubble, using the results of Ref. [10].

2. Pressure effect

Thermodynamics states that a phase change occurs when the chemical potential of a species in the initial phase is higher than the one of the species in the new phase, the difference $\Delta\mu$ being termed as “driving force”. Nucleation, relevant to first-order phase transitions, and recalled in Section 4, depicts the precise mechanism of the formation of the new phase [9] from an initial metastable state. Crystallisation in solution belongs to such transitions, and the driving force $\Delta\mu$ not only increases with solute concentration, but also varies with pressure. This effect may be understood simply as a manifestation of Le Chatelier’s principle: increasing pressure favours the apparition of the densest phase. Therefore if the solute is less dense than the solid phase, a pressure increase will increase supersaturation and favour nucleation of the solid. At constant temperature T , the driving force can be expressed by [9,14,6]:

$$\Delta\mu(T, p) = \Delta\mu(T, p_0) + \int_{p_0}^p (\bar{v}_L(p) - v_S(p_0))_T dp, \quad (1)$$

where $\Delta\mu(T, p_0)$ is the driving force at temperature T and atmospheric pressure p_0 , \bar{v}_L is the specific molecular volume of the solute, and v_S is the molecular volume of the solid. The driving force can be expressed as a function of the supersaturation ratio $S(T, p) = a(T, p)/a_{eq}(T, p)$ where $a(T, p)$ is the activity of the solute (or its concentration in the case of dilute solutions), and $a_{eq}(T, p)$ its equilibrium value at temperature T and pressure p :

$$\Delta\mu(T, p) = k_B T \ln S(T, p), \quad (2)$$

where k_B is the Boltzmann constant.

Further assuming that $\bar{v}_L - v_S$ is independent of p , from (1), the expression of supersaturation as a function of temperature and pressure reads:

$$S(T, p) = S(T, p_0) \exp \left[\frac{\bar{v}_L - v_S}{k_B T} (p - p_0) \right]. \quad (3)$$

The latter expression can be understood as follows: for species with property $\bar{v}_L - v_S > 0$, thus more dense in solid form than in solute form, supersaturation increases with pressure, so that an increase of the latter would favour nucleation. The pressure effect invoked to explain nucleation enhancement by cavitation originates therefore from the large pressure occurring in the liquid at the end of the bubble collapse.

To further quantify the latter point, we consider a standard value $\bar{v}_L - v_S = 0.01 \text{ nm}^3$. In this case, the driving force for a given activity a at 0.1 MPa (that is in ambient conditions) is found to be the same as the driving force for an activity $a/10$ at 950 MPa. This means that, if such pressures could be reached, the same nucleation rates could be obtained with a solution more diluted than in ambient conditions. To assess the latter point, a simulation of a typical inertial cavitation bubble shows that the pressure in the liquid near a collapsing bubble may indeed reach up to 1 GPa (Fig. 1). The model used is described elsewhere [15,12,10]

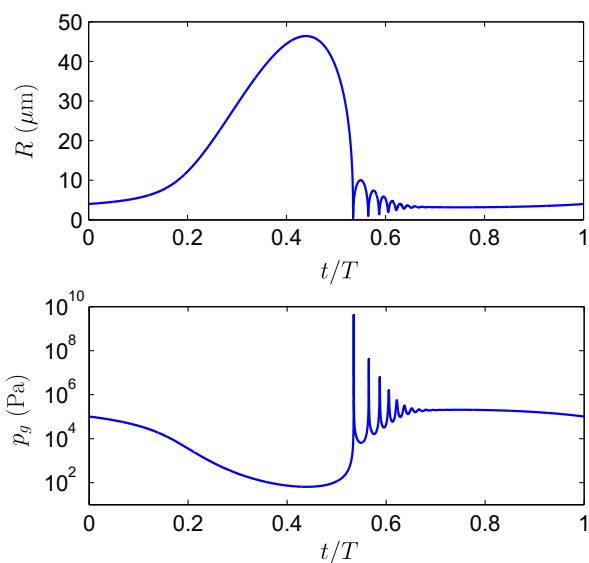


Fig. 1. Simulation of an inertial cavitation air bubble. Top: radius interface of bubble on one acoustic period, for a field amplitude of 130 kPa, $R_0 = 4 \mu\text{m}$ and frequency of 20 kHz. In the bottom, pressure in the liquid at the bubble interface.

and has been validated by single-bubble sonoluminescence experiments.

Thus, the pressure effect could favour nucleation in the case where $\bar{v}_L - v_S > 0$. This is the case for ammonium sulphate, which sono-crystallisation was studied by Virone et al. [6]. Using an estimate of the collapse pressure of the cavitating bubbles, they made an attempt to calculate the nucleation rate using the above theory, assuming that homogeneous nucleation occurs, and the calculated induction times were compared to the values measured in a specially designed cavitator. They found a poor agreement between the experimental and calculated induction times, which was attributed, among other reasons, to the hypothesis of stationary nucleation and the limitations of the detection method.

Besides, strong reduction of induction times have been observed for different crystals under ultrasound: potassium sulphate [2] and glycine [11], which conversely, are less dense in the solid phase than in solute form ($\bar{v}_L - v_S < 0$). The positive results obtained with such crystals demonstrate that the pressure effect alone cannot explain all experimental results.

Fig. 2 displays the relative solubility of different salts as a function of pressure. It is seen for example that the solubility of ammonium nitrate is lower at high pressure than in ambient conditions, while the opposite holds for potassium sulphate. Zinc sulphate

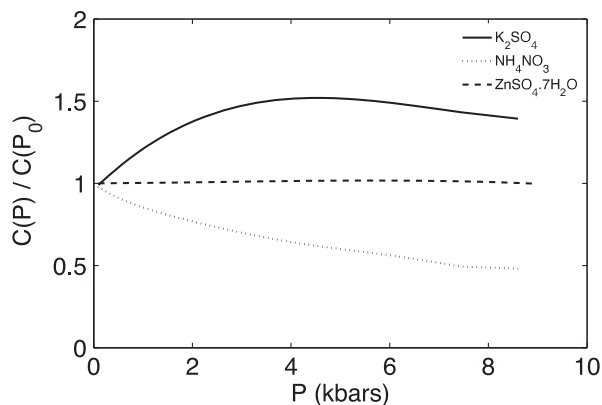


Fig. 2. Relative solubility of different salts as a function of pressure from [17].

heptahydrate presents the interesting feature that its solubility in water is pressure-independent over a large pressure range [16,17], which means that the molecular volumes of solute and solid are very close ($\bar{v}_L - v_S = 0$). Thus, this salt is a good candidate to confirm or disprove the pressure effect on crystals nucleation. We therefore carried out experiments of $\text{ZnSO}_4 \cdot 7\text{H}_2\text{O}$ crystallisation, under silent conditions and in the presence of ultrasound.

3. Experimental

3.1. Solubility

An excess of solid (zinc sulphate heptahydrate, Riedel-de Hain purity min 99%) was added to a known mass of ultra pure water (18.2 MΩ cm) at constant temperature. The conductivity of solution was monitored. The liquid-solid equilibrium was considered to be reached when the conductivity did not vary noticeably. A quantity of 4 g of suspension was taken off and filtered (0.45 μm). The solvent (water) was evaporated from solution at ambient temperature in order to know the amount of salt dissolved, and to preserved the hydration of salt. Besides, X-ray diffraction has been made on some dry samples in order to make sure that the solid phase was indeed the heptahydrate form of zinc sulphate. The main peaks examined for $\text{ZnSO}_4 \cdot 7\text{H}_2\text{O}$ were $2\theta = 20^\circ$, 21° , 34.1° and 35° [18].

The solubility of $\text{ZnSO}_4 \cdot 7\text{H}_2\text{O}$ in water has been measured at different temperatures. The plus signs in Fig. 3 represent our own experimental values of solubility, expressed in mass fractions ω in g of hydrated salt/g of solution, measured at different temperatures, along with solubility data found in the literature. Experiments have been repeated three times, yielding an experimental error on ω_{eq} ranging between 10^{-4} and 9×10^{-4} g/g, depending on the temperature (note that the plus signs in Fig. 3 appear thick because all the measurements at the same temperature are displayed).

As can be seen in Fig. 3, the solubility of $\text{ZnSO}_4 \cdot 7\text{H}_2\text{O}$ in water increases as a function of temperature, and our experimental solubilities are in reasonable agreement with the results of the literature [19–21], although our values are systematically lower than the latter. We have no explanation for this discrepancy, and feel that using our own solubility measurements on the salt we used in crystallisation experiments is the safest method.

In order to calculate the supersaturations involved in our crystallisation experiments, an analytical expression of $\omega_{\text{eq}}(T)$ is

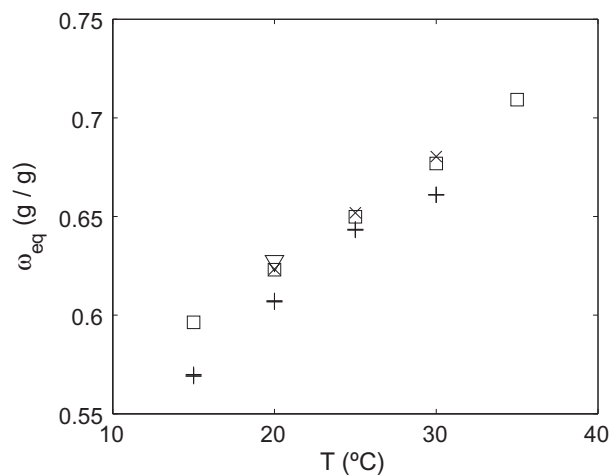


Fig. 3. Solubility of $\text{ZnSO}_4 \cdot 7\text{H}_2\text{O}$ as a function of temperature. Triangles: [19]; × signs: [20]; squares: [21]; + signs: our experimental data.

needed. Since those experiments are performed for temperatures between 24 °C and 25 °C, we chose to use a linear fit between the three solubilities measured at 20 °C and the three ones measured at 25 °C. We obtain:

$$\omega_{\text{eq}} \text{ (g/g)} = 7.26 \cdot 10^{-3} T \text{ (}^\circ\text{C)} + 0.4618 \quad (4)$$

with an error lower than 3×10^{-4} g/g for temperatures ranging between 24 °C and 25 °C.

3.2. Measurement of induction time

The experimental apparatus used for the determination of induction time is represented in Fig. 4. A thermostated vessel (500 ml) was stirred with a magnetic stir bar at a constant rotation speed of about 500 rpm. Ultrasound was applied at the top of the liquid by a stainless tip transducer with a diameter of 1.1 cm, immersed at a 1.5 cm depth in the vessel. Two ultrasonic power levels were used, corresponding to dissipated powers of 16 and 30 W, measured in water by the calorimetric method at 25 °C. The solution temperature is measured with an instrumental resolution of 0.01 °C.

Before each experiment, in order to dissolve all the solid, suspensions were heated to a temperature higher by 8 °C than the saturation temperature during 1 hour. The saturation temperature ranged between 28 °C and 32 °C. Then, the solution was rapidly cooled to a temperature around 25 °C. Ultrasound is applied at the end of the cooling phase (≈ 720 s). The appearance of crystals was detected by the sudden increase of temperature. The induction time t_{ind} is defined as the time elapsed between the creation of supersaturation and the appearance of crystals. The induction time is measured as soon as the temperature 25 °C is reached. At the end of each experiment, the suspension was filtrated (0.45 μm), and the crystals were dried at room temperature, in order to avoid destruction of the crystalline structure by heating.

3.3. Results and discussion

Figs. 5 and 6 display examples of time variations of the solution temperature in silent conditions, and under insonification, respectively (note the different scales on the time-axis). The different steps are clearly visible on both figures: heating, cooling, and plateau at crystallisation temperature. The increase of temperature observed on the plateau corresponds to the appearance of the solid phase.

The variation of induction time with absolute supersaturation is summarised in Fig. 7 and Tables 1 and 2. The absolute supersaturation $\Delta\omega = \omega - \omega_{\text{eq}}(T)$ is calculated as the difference between the initial, and saturation mass fractions at the crystallisation temperature. The absolute error on $\Delta\omega$ is the sum of the absolute errors on ω and ω_{eq} and reaches 5×10^{-4} for all points.

We obtained the same type of curve with and without ultrasound. The induction time decreases when absolute supersatura-

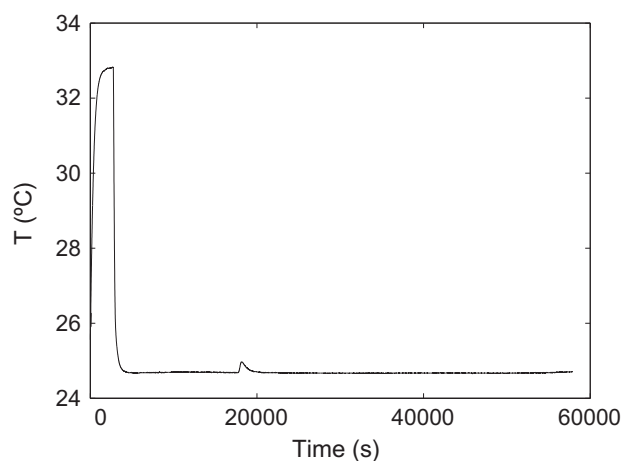


Fig. 5. Experiment without ultrasound, $\Delta\omega = \omega - \omega_{\text{eq}}(T) = 0.0305 \pm 5 \times 10^{-4}$ g/g, cooling time = 720 s, temperature of dissolution = 36 °C, $t_{\text{ind}} = 13740$ s, temperature of crystallisation = 24.70 °C.

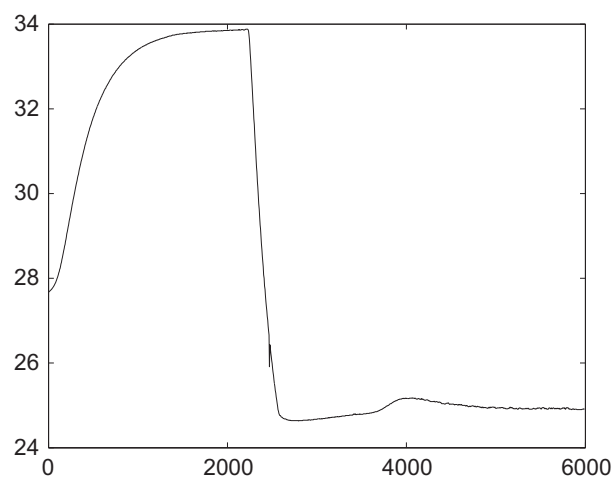


Fig. 6. Experiment with ultrasound, $\Delta\omega = \omega - \omega_{\text{eq}}(T) = 0.0317 \pm 5 \times 10^{-4}$ g/g, cooling time = 720 s, temperature of dissolution = 36 °C, dissipated power = 16 W, $t_{\text{ind}} = 960$ s, temperature of crystallisation = 24.68 °C.

tion increases. This behaviour agrees with classical results on crystallisation. However, we can observe that ultrasound has a significant effect on induction time, especially at low supersaturation, where the induction time can be reduced by one order of magnitude. This effect is less significant at high supersaturation, since nucleation is very fast anyway in this case. Besides, it was checked that the X-ray diffraction patterns of the powders crystallised without and with ultrasound were the same, and correspond to the same orthorhombic structure.

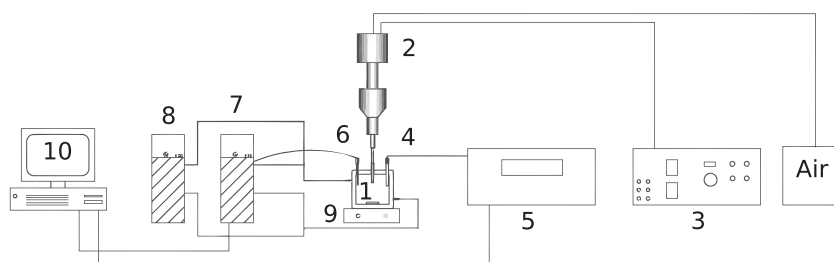


Fig. 4. Experimental set-up: (1) Thermostated reactor; (2) sonotrode; (3) generator of ultrasound; (4) conductimetry probe; (5) conductimeter; (6) temperature probe; (7 and 8) cooling baths; (9) magnetic stirrer; and (10) computer.

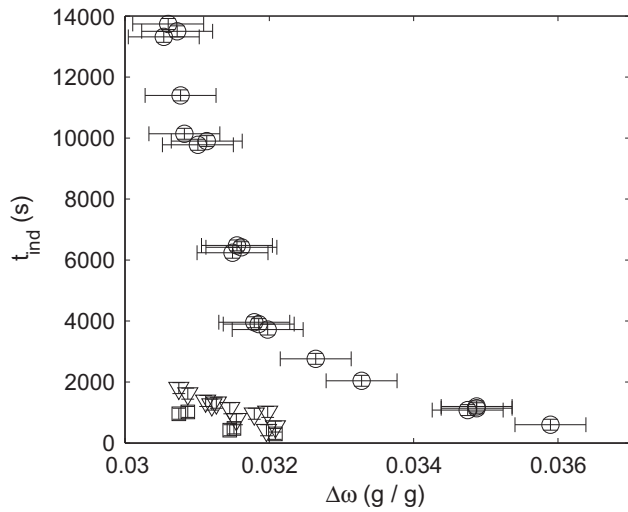


Fig. 7. Induction time of $\text{ZnSO}_4 \cdot 7\text{H}_2\text{O}$ as a function of absolute supersaturation in silent conditions (circles), insonification with $P = 16$ W (triangles) and insonification with $P = 30$ W (squares). The horizontal errorbars have been skipped for the points with insonification, in order to make the figure readable. They are equal to the ones for the points in silent conditions. The vertical errorbars are represented for all points.

Table 1
Results of all experiments without ultrasound: induction time as function of absolute supersaturation $\Delta\omega$.

ω (g/g)	$\Delta\omega$ (g/g)	Temperature of crystallisation (± 0.01 °C)	t_{ind} (s)
($\pm 2 \times 10^{-4}$)	($\pm 5 \times 10^{-4}$)		(± 180 s)
<i>Without ultrasound</i>			
0.6649	0.0314	24.70	6240
0.6649	0.0315	24.69	6480
0.6649	0.0316	24.68	6420
0.6651	0.0319	24.65	3720
0.6651	0.0317	24.68	3960
0.6651	0.0318	24.67	3900
0.6664	0.0326	24.60	2760
0.6665	0.0332	24.67	2040
0.6645	0.0308	24.75	10,140
0.6645	0.0311	24.70	9900
0.6645	0.0310	24.72	9780
0.6640	0.0305	24.71	13,320
0.6640	0.0305	24.70	13,740
0.6640	0.0307	24.68	13,500
0.6643	0.0307	24.73	11,400
0.6690	0.0358	24.65	600
0.6683	0.0347	24.72	1080
0.6683	0.0348	24.70	1140
0.6683	0.0348	24.70	1200

The results obtained are very similar to the ones obtained for potassium sulphate [2], glycine [11] or ammonium sulphate [6]. Thus, it appears that the ability of cavitation to accelerate nucleation at low supersaturation is similar for crystals which solubility either increases with pressure, or decreases with pressure, or is pressure-independent. This generic tendency questions therefore the reality of the pressure effect on nucleation in solutions.

One may argue however, that the nucleated crystals could be a different polymorph, which solubility decreases with pressure, which would be further transformed in some way to the one observed at the end of the experiment. This cannot be completely excluded since our experimental method clearly does not allow to observe the early stages of nucleation, and that various phenomena may have already occurred when we detect the first crystals. This is by the way the scenario classically mentioned for ice nucleation under ultrasound, where high pressure phases of ice, which are denser than liquid water, are the polymorphs suspected to nucle-

Table 2
Results of all experiments with ultrasound: induction time as function of absolute supersaturation $\Delta\omega$, for different dissipated powers.

ω (g/g)	$\Delta\omega$ (g/g)	Temperature of crystallisation (± 0.01 °C)	t_{ind} (s)
($\pm 2 \cdot 10^{-4}$)	($\pm 5 \cdot 10^{-4}$)		(± 180 s)
<i>With ultrasound P = 16 W</i>			
0.6649	0.0308	24.8	1620
0.6649	0.0307	24.82	1800
0.6649	0.0311	24.76	1380
0.6643	0.0312	24.65	1320
0.6643	0.0314	24.62	1140
0.6643	0.0312	24.66	1260
0.6651	0.0319	24.65	1020
0.6651	0.0315	24.72	780
0.6651	0.0317	24.68	960
0.6654	0.0320	24.68	540
0.6654	0.0319	24.70	420
<i>With ultrasound P = 30 W</i>			
0.6649	0.0308	24.80	1020
0.6649	0.0307	24.82	960
0.6643	0.0315	24.65	480
0.6643	0.0314	24.62	420
0.6654	0.0320	24.68	300

ate by the pressure effect, and further grow and transform into ice I [22]. However, although classically mentioned, there is no direct experimental proof of this scenario. Furthermore, it strongly relies on the existence of a polymorph which solubility is lower at high pressure, which, to our knowledge, is not the case for K_2SO_4 for example. The universality of the effect of cavitation on various salts suggests therefore that the pressure effect is not generic enough to be the only mechanism involved, and that a more generic physical mechanism should be invoked.

For this reason, after recalling the main lines of the classic nucleation theory, we examine hereafter the present results in the light of the segregation theory [10,13].

4. Theory

4.1. Nucleation

The formation of crystals in liquid solutions begins with nucleation. The classical nucleation theory describes nucleation as successive attachments and detachments of single molecules, denoted as “monomers”, to form clusters of different sizes [9,14], having the density of the solid. The work $W(n)$ necessary to form a cluster containing n monomers is given by the difference between the free energy of the system in its initial and final state, and is the sum of two competitive energy terms:

$$W(n) = -n\Delta\mu + \gamma c(nv_s)^{2/3}, \quad (5)$$

where $\Delta\mu$ is the driving force given by (1), γ is the solid-liquid interfacial tension, v_s the molecular volume of the solid, and c is a shape factor [$(36\pi)^{1/3}$ in the case of a spherical cluster]. The negative volume energy term represents the natural tendency of a cluster to appear in the metastable solution, whereas the positive energy term represents the interfacial energy necessary to form the cluster interface. The competition of these two energy contributions lead to a maximum W^* of the work $W(n)$ for a value $n = n^*$, known as “critical cluster” or “nucleus”, the maximum work W^* thus representing the energy barrier for nucleation to occur. Assuming spherical clusters, n^* and W^* are respectively given by:

$$n^* = \frac{8c^3 v_s^2 \gamma^3}{27(k_B T)^3 \ln^3 S} \quad (6)$$

and

$$W^* = \frac{4c^3 v_s^2 \gamma^3}{27(k_B T)^2 \ln^2 S}. \quad (7)$$

The nucleation kinetics may be obtained by assuming that the cluster population evolves by successive attachments and detachment process [9], represented by the pseudo-chemical reactions:



The kinetics of the elementary direct and inverse reactions (8) is assumed to be first-order against each reactive and product. Denoting $Z_n(t)$ the time-varying concentration in clusters of size n , k_{nm} the reaction rate of the direct reaction, and l_{mn} the rate of the inverse reaction, the reaction (8) contributes to the rate of production of Z_n as:

$$\frac{dZ_n}{dt} = -k_{nm}Z_nZ_{m-n} + l_{mn}Z_m. \quad (9)$$

The attachment and detachment frequencies k_{nm} and l_{mn} depend on the attachment mechanism, but are not independent. Elementary reactions (9) are generally recast by using the ‘‘equilibrium’’ concentration of the clusters C_n determined by thermodynamical considerations, by considering the solution as an ideal mixture of clusters of all sizes:

$$C_n = C_0 \exp\left[-\frac{W(n)}{k_B T}\right], \quad (10)$$

where C_0 is the molecular concentration of possible nucleating sites, generally evaluated by $1/v_s$. Introducing C_n in (9), one obtains the equilibrium condition:

$$-k_{nm}C_nC_{m-n} + l_{mn}C_m = 0, \quad (11)$$

which allows to express the detachment constants l_{mn} once the attachments constants k_{nm} are known. It should be recalled that an equilibrium concentration of clusters does not make sense in the case of a super-saturated solution, but it constitutes an elegant turnaround to avoid the estimation of detachment frequency. A deeper discussion of these aspects is out of the scope of this paper, and we refer the interested reader to Ref. [9] for a detailed consideration of these theoretical issues.

Accounting for all the reactions starting at, or reaching the cluster size (n), the ordinary differential equation (ODE) governing the production-rate of (n)-clusters reads [9]:

$$\frac{dZ_n}{dt} = \frac{1}{2} \sum_{m=1}^{n-1} k_{mn} \left(Z_{n-m}Z_m - C_{n-m}C_m \frac{Z_n}{C_n} \right) - \sum_{m=n+1}^M k_{nm} \left(Z_{m-n}Z_n - C_{m-n}C_n \frac{Z_m}{C_m} \right). \quad (12)$$

More progress can be made by noting that, since clusters (n) are much less numerous than monomers, it is generally considered that the only attachments likely to occur are the ones between (n)-clusters and monomers [so that $m = n + 1$ in Eq. (8)], disregarding direct attachments between (n) and ($m - n$). In this case the governing set of equations (12) can be considerably simplified. Furthermore, considering the cluster-size n as a continuous variable, the sets transforms into a partial-differential equation for $Z_n(t)$, which is more amenable to analytical solutions [14,9]. In particular, a stationary solution X_n of the governing equation can be sought by setting $\partial Z_n(t)/\partial t = 0$ and one obtains:

$$X_n = \frac{1}{2} C_n [1 - \operatorname{erf}(\pi^{1/2} z(n - n^*))] \quad (13)$$

where z is the so-called Zeldovich factor:

$$z = \frac{3}{4\sqrt{\pi}} \left(\frac{k_B T}{c v_s^2 \gamma} \right)^{3/2} \ln^2 S,$$

measuring the narrowness around the critical cluster of the energy peak defined by (7). This solution is displayed in Fig. 8 for one of the lowest supersaturation $\Delta\omega = 0.0305$ g/g (corresponding to the leftmost points of Fig. 7), yielding a supersaturation ratio $S = 1.222$ and a critical cluster $n^* = 117$. Section A details the calculation of supersaturation ratio from ions activities. The vertical dashed-line materialises the critical cluster size n^* . This graph can be readily interpreted as follows: below the critical size, the detachment processes are dominant, so that the concentration in small clusters is almost the equilibrium one. Above n^* the attachment process become preponderant, and the large clusters grow rapidly, so that their concentration is low. The critical cluster thus appears as a ‘‘bottleneck’’ on the nucleation process, as a result of the energy barrier located there and quantified by Eq. (7).

Then, from the analytical solution (13), the global stationary nucleation rate J_s , that is, the number of critical clusters formed per unit-time and unit-volume, can be obtained by evaluating the number of nuclei crossing the critical size per unit-time, and one finally obtains [9]:

$$J_s = A \exp\left(-\frac{B}{T^3 \ln^2 S}\right), \quad (14)$$

where A is a quantity almost independent of the supersaturation ratio S , and B reads

$$B = \frac{4c^3 v_s^2 \gamma^3}{27k_B^3}. \quad (15)$$

The induction time can be related to the nucleation rate J_s by $t_{\text{ind}} = 1/(J_s V)$, where V is the volume of the solution. This result, along with Eq. (14), is classically used to determine the liquid-solid interfacial energy γ from induction-time measurements, by fitting $\ln(t_{\text{ind}})$ vs. $1/(T^3 \ln^2 S)$ with a straight line, which slope yields B and therefore γ .

It may be argued however, that during the induction time we measure, nucleation is not the only phenomenon involved but that growth can also occur. In this case, matching t_{ind} with $1/(J_s V)$ is no longer justified and the theory must be enhanced in order to also account for growth. The methodology is more complex in this case, because numerous growth-mechanisms can be involved. To assess the latter point, we followed the method of Ref. [23], by considering separately all possible growth mechanism, each one yielding theoretically a specific functional dependence between rescaled functions of the induction time t_{ind} and the supersaturation S . The most probable mechanism is then elected by choosing the best correlation with the experimental points among all the potential solutions.

We performed such an extended study, and a summary is presented in Section B. The conclusion is that a pure nucleation process still remains the best candidate, so that growth mechanisms are thought to be of lower importance, at least in the early stages of the solid formation we consider here. Of course, the study of Section B is only made on the experimental points without ultrasound, since the underlying theories are only valid in this case. Thus, an influence of the cavitation bubbles on growth-processes cannot be definitely excluded, and considering only their effect on nucleation, as done below in this paper, should be considered as a working hypothesis rather than an established fact.

The linear fit between $\ln(t_{\text{ind}})$ and $1/(T^3 \ln^2 S)$ is displayed in Fig. 9, and yields $\gamma = 3.21 \pm 0.04$ mJ/m².

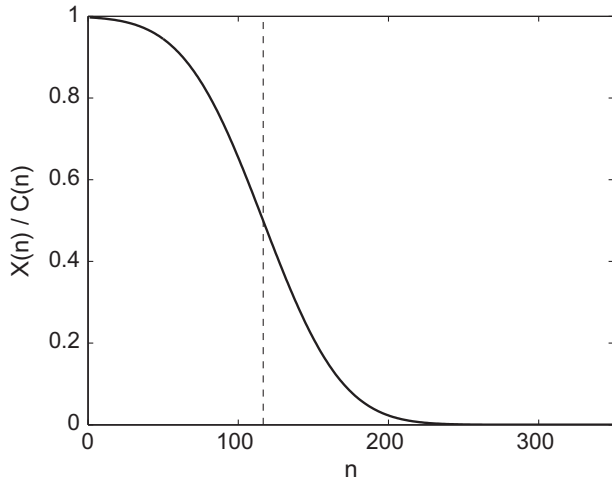


Fig. 8. Concentration of clusters for stationary nucleation. $\Delta\omega = 0.0305$ g/g, $S = 1.222$, $n^* = 117$.

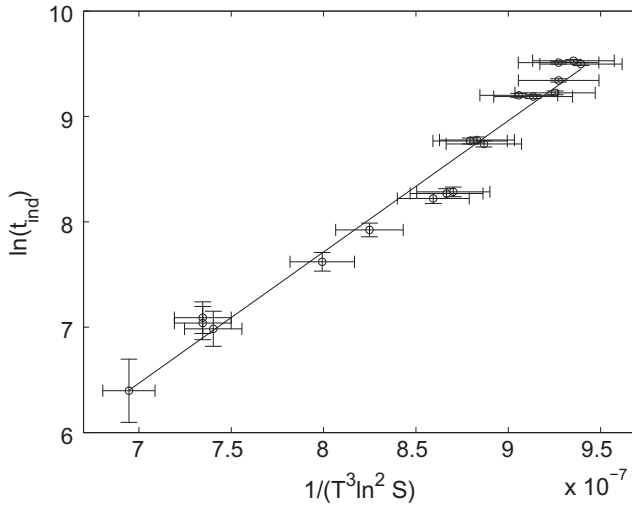


Fig. 9. Logarithm of the experimental induction time vs. $1/(T^3 \ln^2 S)$. The slope allows to calculate the interfacial energy γ through Eq. (15). The errorbars represent the experimental errors.

The value of the interfacial energy γ is crucial since it has a huge influence on all quantities calculated within nucleation theory, especially n^* . Thus, in order to check the correctness of our experimentally determined value of γ , we compare the latter to the well-known semi-empirical relation [24,14]:

$$\gamma \frac{v_S^{2/3}}{k_B T} = K \ln \frac{C_S}{C_{eq}}, \quad (16)$$

where C_S is the molar concentration of the solid phase, C_{eq} is the molar equilibrium concentration of the solute, and K a multiplicative factor, which recommended value ranges between 0.3 and 0.5. Our experimental value of γ casts well in Eq. (16) with a numerical factor $K = 0.423 \pm 0.005$.

With the value of γ at hand, it is possible to evaluate the size of the critical cluster n^* by Eq. (6) for each supersaturation value. The result is displayed in Fig. 10. In the range of supersaturations used in our experiments [1.222, 1.263], n^* ranges between 74 and 117.

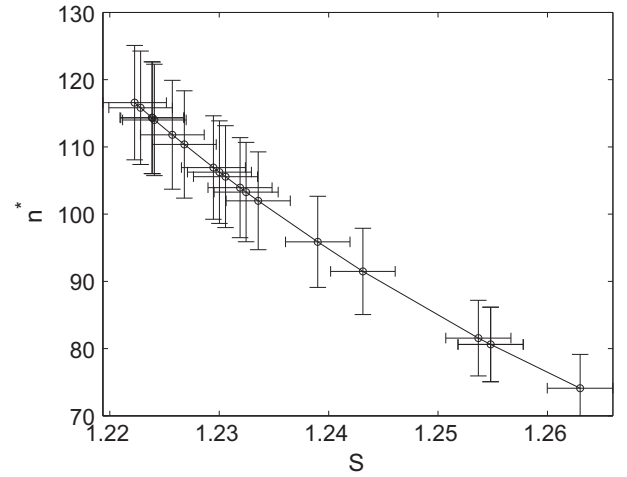


Fig. 10. Size of the critical cluster as a function of the supersaturation ratio S , calculated from Eq. (6). The points correspond to our experiments. The horizontal errorbars originate from the experimental errors on ω and ω_{eq} , and the vertical errorbars originate both from the experimental errors on ω and ω_{eq} and the uncertainty on the determination of γ , when using Eq. (6).

4.2. Segregation theory

As an alternative to the hypothesis of pressure effect, which, as shown in Section 3.3, should be discarded for zinc sulphate, we recently proposed that nucleation enhancement by ultrasound could be caused by a direct effect of cavitation on the agglomeration process of the clusters [10,13].

The basic mechanism is that at the end of the collapse, the fast inward motion of the mixture is stopped violently by the gas recompression in the bubble, yielding a huge outward acceleration (typically 10^{11} g). If the clusters are more dense than the surrounding liquid, which is generally the case for crystallisation in solutions, they undergo an inward drift motion relative to the liquid, and become over-concentrated near the bubble wall for a very short time (typically 1 ns). This forced diffusion of two species of different densities in a pressure gradient physics is somewhat similar to the one underlying ultra-centrifugation, and is known as “pressure diffusion”.

This segregation effect around a given cavitation bubble has been quantified analytically in Ref. [10] by a perturbation method. The theory allows to calculate the spatio-temporal variations of the concentration in any species of known density and diffusion coefficient (or hydrodynamic radius), once the bubble radial dynamics is known. On this basis, it has been suggested in Ref. [13] that in a metastable solution, this effect should over-concentrate the clusters near the bubble wall at each collapse, therefore favouring their direct collision, and enhancing the global nucleation kinetics.

To further quantify this hypothesis, we evaluate the concentration of clusters as they become segregated from the liquid by the bubble motion, in the conditions of the above crystallisation experiments. We consider the same supersaturation as in Fig. 8, yielding a critical cluster size $n^* = 117$, and quantify the concentration of clusters which size ranges between 1 and $3n^*$, near a typical inertial cavitation bubble. We assume an air bubble of ambient radius $R_0 = 4$ μm in water, driven by a far sound field of the form $p_\infty(t) = p_0[1 - p_a^* \sin(2\pi ft)]$, where p_0 is the ambient static pressure, $f = 20$ kHz the frequency, and p_a^* the dimensionless driving amplitude. Inertial cavitation, involving explosive growth and collapse of the bubble, occurs slightly above $p_a^* = 1$ [25,26], and the steady-state dynamics is calculated using the model of Ref. [15].

The segregation theory developed in Ref. [10] shows that the concentration of the densest species of a mixture at the bubble wall reads:

$$C(t) = C_\infty (C_{av}^* + C_{osc}^*(t)), \quad (17)$$

where C_∞ is the concentration of the species in the undisturbed liquid, and the expressions of C_{av}^* and C_{osc}^* depend on the mixture and the bubble-dynamics:

$$C_{av}^* = \exp(\beta I), \quad (18)$$

$$C_{osc}^*(t) = \exp(\beta I) \frac{-\beta}{Pe^{1/2}} g(t), \quad (19)$$

where the quantity I involves averages of some functionals of the bubble radius, and, in the range of parameters considered here, is small enough to have $e^{\beta I} \simeq 1$. The function $g(t)$ can be evaluated once the bubble dynamics is known, and is typically a narrow positive pulse centred near the bubble collapse. Of special interest is the maximum value g_{max} reached by $g(t)$ near the bubble collapse. The parameter β basically represents the difference in the densities of the two segregated species. In the present case, for of cluster of size n , it reads:

$$\beta_n = \frac{1}{2} R_0^2 (2\pi f)^2 \frac{v_s}{k_B T} (\rho - \rho_s) n, \quad (20)$$

where R_0 is the bubble ambient radius, f the ultrasound frequency, ρ the density of the solution, and ρ_s the density of the solid, so that β is negative in the present case since the solid phase is denser than the liquid (as is generally the case for crystallisation in solution).

The Péclet number Pe appearing in Eq. (19) is defined by:

$$Pe_n = \frac{R_0^2 (2\pi f)}{D_n}, \quad (21)$$

where D_n is the diffusion coefficient of (n)-clusters in the solution. It can be evaluated by the Stokes–Einstein relation, assuming spherical clusters:

$$D_n = \frac{k_B T}{6\pi(3v_s n / (4\pi))^{1/3} \eta}, \quad (22)$$

where η is the liquid viscosity.

We assume that far from the bubbles, stationary nucleation takes place so that their undisturbed concentration $C_\infty(n)$ is X_n given by Eq. (13) (see Fig. 8), and we calculate the concentration of the clusters at the bubble wall $X_{seg}(n) = X_n \times \max_t C_{osc}^*(n, t)$ from Eqs. (19)–(22), for each size n . The result is displayed in Fig. 11 for various amplitudes of the driving acoustic pressure. The vertical dashed line denotes the size of the critical cluster. It is seen that segregation over-concentrates all the clusters, especially in a region below the critical cluster, up to more than 20 times for an acoustic pressure of 1.5 bar (upper curve). The concentration in clusters for stationary nucleation far from the bubble (Eq. (13) and Fig. 8) is recalled in dashed line for comparison.

We suggest that this transitory over-concentration may enhance drastically the process of cluster growth not only by monomer aggregation, but may also favour direct aggregation of multimers, generally negligible in silent nucleation. Looking at Fig. 11, it is seen for example that near a cavitation bubble driven at 1.5 bar, the concentration of the 80-mers clusters is multiplied by about 25, which multiplies their mutual collision probability by 625. Segregation makes therefore direct aggregation processes more probable, which may lead to a global enhancement of nucleation process.

Applying this theory to other solutions yields similar results [11]. The segregation theory relies in fact only on the hypothesis that the solid phase is denser than the solution, which is generally

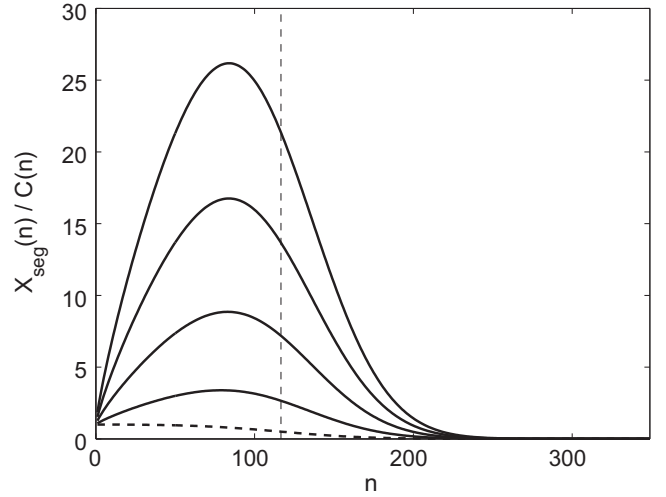


Fig. 11. Solid lines: concentration of clusters near a 4 μm air bubble driven at 20 kHz, at the end of the collapse; from bottom to top: $p_a = 1.2, 1.3, 1.4, 1.5$. The dashed line represents the concentration for stationary nucleation far from the bubble (same curve as Fig. 8). The vertical dashed line denotes the critical cluster size. $S = 1.222$, $n^* = 117$.

the case for solution crystallisation, and applies indifferently to potassium sulphate, ammonium sulphate or glycine. The present theory presents therefore the advantage to be compatible with all the experimental results mentioned above. The missing link with macroscopic results is the calculation of a macroscopic induction-time, based on this theory. This would require to solve the equations of transitory nucleation like, Eq. (12), taking into account the periodic transitory over-concentration peaks over the whole range of cluster sizes. This theoretical problem is currently under consideration for a single-bubble. It should also be noted that there is yet no direct experimental validation or invalidation of the segregation effect, although its theoretical basis is well-established. Work is also in progress in this way.

Finally, we emphasise that the quantitative extrapolation of this single-bubble theory to observable macroscopic effects in multi-bubble fields is difficult, for the same reasons as the ones mentioned for the pressure effect [6], or any other proposed microscopic mechanism. Indeed, in the absence of a reliable theory yielding the size-distribution and spatial repartition of the cavitation bubbles, no precise extrapolation can be done. This issue is in fact more general than sono-crystallisation, and is also relevant to sonochemistry, and any cavitation-enhanced process.

5. Conclusions

Past results on sono-crystallisation of species less dense in solid form than in solute form have cast some doubts on the nucleation enhancement by the high pressures appearing near a cavitation bubble. The present results on zinc sulphate show that, although its solubility is pressure-independent, the induction time is drastically reduced by ultrasound. Instead, we have shown that an interpretation by the segregation theory remains semi-quantitatively plausible, and shows that the over-concentration of the clusters around the critical nucleus near collapsing bubbles may reach more than one order of magnitude. This enhances the direct aggregation probability between near-critical clusters by more than two orders of magnitude, and may therefore accelerate the global nucleation process. A more precise quantification of this process is under consideration.

Acknowledgment

The authors acknowledge the Institut Carnot-MINES, France, for financial support.

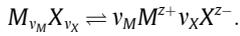
Appendix A. Calculation of the supersaturation ratio

In the molality (mole of solute per kg of "free" water) scale, the activity of salt $M_{v_M}X_{v_X}$ in solution can be expressed by the following equation:

$$a_{MX} = m_{MX}\gamma_{MX}, \quad (\text{A.1})$$

where m_{MX} and γ_{MX} represents the molality and the activity coefficient respectively.

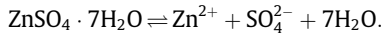
In the aqueous solution, the dissociation of salt $M_{v_M}X_{v_X}$ can be expressed by:



The ionic activity for each component i can be written as:

$$a_i = m_i \gamma_i. \quad (\text{A.2})$$

For an hydrate salt, such as $\text{ZnSO}_4 \cdot 7\text{H}_2\text{O}$, the dissociation can be expressed by:



Therefore, the expression of the supersaturation ratio of $\text{ZnSO}_4 \cdot 7\text{H}_2\text{O}$ can be written as:

$$S = \frac{a_{\text{Zn}^{2+}}^{2} a_{\text{SO}_4^{2-}}^{2} a_{\text{H}_2\text{O}}^7}{a_{\text{Zn}^{2+},\text{eq}}^2 a_{\text{SO}_4^{2-},\text{eq}}^2 a_{\text{H}_2\text{O},\text{eq}}^7}. \quad (\text{A.3})$$

Using Eq. (A.2), Eq. (A.3) can be expressed as:

$$S = \frac{m_{\text{Zn}^{2+}}^{2+\gamma} \gamma_{\text{Zn}^{2+}} m_{\text{SO}_4^{2-}}^2 \gamma_{\text{SO}_4^{2-}} a_{\text{H}_2\text{O}}^7}{m_{\text{Zn}^{2+},\text{eq}}^2 \gamma_{\text{Zn}^{2+},\text{eq}}^2 m_{\text{SO}_4^{2-},\text{eq}}^2 \gamma_{\text{SO}_4^{2-},\text{eq}}^2 a_{\text{H}_2\text{O},\text{eq}}^7}. \quad (\text{A.4})$$

The mean molal activity coefficient (noted γ_{\pm}) can be calculated from the ionic activity coefficient using:

$$\gamma_{\pm}^{v_M+v_X} = \gamma_{M^{z^+}}^{v_M} \times \gamma_{X^{z^-}}^{v_X}, \quad (\text{A.5})$$

where v_M and v_X are the stoichiometric coefficients of cation and anion respectively.

Using this mean coefficient, Eq. (A.4) becomes:

$$S = \frac{m_{\text{ZnSO}_4}^2 \gamma_{\pm}^2 a_{\text{H}_2\text{O}}^7}{m_{\text{ZnSO}_4,\text{eq}}^2 \gamma_{\pm,\text{eq}}^2 a_{\text{H}_2\text{O},\text{eq}}^7}. \quad (\text{A.6})$$

The molality is calculated using our own experimental values of the mass fractions, summarised in Table 1, by:

$$m_{\text{ZnSO}_4} = \frac{1000\omega/M_{\text{ZnSO}_4 \cdot 7\text{H}_2\text{O}}}{1 - \omega M_{\text{ZnSO}_4}/M_{\text{ZnSO}_4 \cdot 7\text{H}_2\text{O}}}, \quad (\text{A.7})$$

where $M_{\text{ZnSO}_4 \cdot 7\text{H}_2\text{O}}$ and M_{ZnSO_4} are the molar mass of $\text{ZnSO}_4 \cdot 7\text{H}_2\text{O}$ and ZnSO_4 respectively.

Introducing Eq. (A.7) in Eq. (A.6), the supersaturation S now reads:

$$S = \left(\frac{\omega}{\omega_{\text{eq}}} \right)^2 \left(\frac{1 - \omega_{\text{eq}} M_{\text{ZnSO}_4}/M_{\text{ZnSO}_4 \cdot 7\text{H}_2\text{O}}}{1 - \omega M_{\text{ZnSO}_4}/M_{\text{ZnSO}_4 \cdot 7\text{H}_2\text{O}}} \right)^2 \left(\frac{\gamma_{\pm}}{\gamma_{\pm,\text{eq}}} \right)^2 \frac{a_{\text{H}_2\text{O}}(\omega)}{a_{\text{H}_2\text{O}}(\omega_{\text{eq}})}. \quad (\text{A.8})$$

The value of γ_{\pm} is obtained by using a modified Pitzer equation, following Ref. [27].

The water activity $a_{\text{H}_2\text{O}}(\omega)$ can be related to the osmotic coefficient of water ϕ , the molality m_{ZnSO_4} , and the number of moles of ions $\nu = \nu_{\text{Zn}^{2+}} + \nu_{\text{SO}_4^{2-}}$ formed from 1 mol of salt:

$$\ln a_{\text{H}_2\text{O}} = - \frac{\nu \times m \times M_{\text{H}_2\text{O}}}{1000} \phi. \quad (\text{A.9})$$

The osmotic coefficient of $\text{ZnSO}_4 \cdot 7\text{H}_2\text{O}$ is calculated using the same model as for γ_{\pm} [27].

The numerical values obtained for water activities and mean activity coefficients for $\text{ZnSO}_4 \cdot 7\text{H}_2\text{O}$ solution are in good agreement with the results of Ref [28]. The obtained values of supersaturation S , using Eq. (A.8), range between $S = 1.222$ and 1.263 .

Appendix B. Examination of growth processes

The induction time t_{ind} can be represented by the sum of the time necessary for the critical nucleus to be formed, and the time for this nucleus to grow up to a visible size. These two times depend on the nucleation and growth rates of the crystals and the induction time reads [23]:

$$t_{\text{ind}} = \frac{1}{JV} + \left(\frac{\alpha}{a_n J G^{n-1}} \right)^{1/n}, \quad (\text{B.1})$$

where J is the nucleation rate, G the growth rate, a_n the shape factor of nuclei, V the volume and $\alpha = V_m/V$ the volume fraction of nuclei, where V_m is the macroscopic volume of the nuclei.

The induction time measurements are obtained by a method involving three dimensional (3D) growth of the nucleus up to a registrable macroscopic volume V_m , so that n is 4.

Mass transport from solution (diffusion and convection) and surface integration of ions or molecules to crystal lattice (either two-dimensional nucleation or screw dislocation mechanism) are the two consecutive processes occurring during the growth of crystals. In the following, different growing mechanisms have been inspected.

The nucleation rate can be expressed by:

$$J = k_j \exp \left(- \frac{B}{\ln^2 S} \right) \quad (\text{B.2})$$

and the growth rates by:

- 2D nucleation mechanism:

$$G_{2D} = k_G (S - 1)^{2/3} S^{1/3} \exp \left(- \frac{B_{2D}}{3 \ln S} \right). \quad (\text{B.3})$$

- Screw dislocation mechanism:

$$G_{SC} = k_G (S - 1)^2. \quad (\text{B.4})$$

- Growth limited by transport process:

$$G_D = k_G (S - 1). \quad (\text{B.5})$$

The terms B and B_{2D} are respectively proportional to surface energy crystal-solution, γ^3 , and to specific edge energy κ^2 .

For the calculation of induction times, three limiting cases have been studied:

1. $t_j \gg t_g$
2. $t_j = t_g$
3. $t_j \ll t_g$

For these different cases, the temperature has been assumed constant and equal to 25 °C. Each assumption yields an expression

Table B.1

Nucleation and growth models. First colon: hypothesis. Second colon: abscissa of the fit. Third colon: ordinate of the fit. Fourth colon: correlation coefficient.

Model	Abscissa	Ordinate	R ²
(1) $t_j \gg t_g$ mononuclear model	$\frac{1}{\ln^2 S}$	$\ln(t_{\text{ind}})$	0.977
(2) $t_j = t_g$ 2D nucleation growth, polynuclear model	$\frac{1}{\ln S}$	$\ln \left[t_{\text{ind}} S^{1/4} \times (S - 1)^{1/2} \right]$	0.983
(3) $t_j = t_g$ growth by screw dislocation mechanism, polynuclear model	$\frac{1}{\ln^2 S}$	$\ln \left[t_{\text{ind}} \times (S - 1)^{3/2} \right]$	0.972
(4) $t_j = t_g$ Growth limited by transport process, polynuclear model	$\frac{1}{\ln^2 S}$	$\ln \left[t_{\text{ind}} \times (S - 1)^{3/4} \right]$	0.975
(5) $t_j \ll t_g$ 2D nucleation growth	$\frac{1}{\ln S}$	$\ln \left[t_{\text{ind}} S^{1/3} \times (S - 1)^{2/3} \right]$	0.971
(6) $t_j \ll t_g$ growth by screw dislocation mechanism, or growth limited by transport process	$\ln(S - 1)$	$\ln(t_{\text{ind}})$	0.969

with a function F_{ind} dependent on induction time and supersaturation ($F_{\text{ind}} = S^{k_1} (S - 1)^{k_2} t_{\text{ind}}$).

The plot of F_{ind} as a function of $1/\ln S$, $1/\ln^2 S$ or $\ln(S - 1)$ would appear as a straight line (cases 1 and 3–6, Table B.1) and the plot of F_{ind} as a function of $1/\ln^2 S$ as a 2nd order polynomial, if the assumptions were verified.

The different correlation factors obtained are summarised in Table B.1. They are very close. The two highest correlation factors are respectively obtained for the nucleation mononuclear model and the polynuclear nucleation model based on 2D-nucleation growth (0.977 and 0.983). However in the case of polynuclear model, the B_{2D} parameter is found negative which it is physically impossible. The same result was obtained in Ref. [29]. Thus, in this study, the mononuclear model has been chosen and a value of 3.21 mJ/m^2 for the surface energy has been elected.

References

- [1] J.W. Mullin, Crystallization, third ed., Butterworth-Heinemann Ltd., 1993.
- [2] N. Lyczko, F. Espitalier, O. Louisnard, J. Schwartzenruber, Chemical Engineering Journal 86 (2002) 233–241.
- [3] R. Sirinivasan, I. Shirgaonkar, A. Pandit, Separation Science and Technology 10 (1995) 2239–2243.
- [4] H. Li, H.R. Li, Z.C. Guo, Y. Liu, Ultrasonics Sonochemistry 13 (2006) 359–363.
- [5] E. Miyasaka, M. Takai, H. Hidaka, Y. Kakimoto, I. Hirasawa, Ultrasonics Sonochemistry 13 (2006) 308–312.
- [6] C. Virone, H.J.M. Cramer, G.M.V. Rosmalen, A.H. Stoop, T.W. Bakker, Journal of Crystal Growth 294 (2006) 9–15.
- [7] A. Kordylla, S. Koch, F. Tumakaka, G. Schembecker, Journal of Crystal Growth 310 (2008) 4177–4184.
- [8] G. Rucroft, D. Hipkiss, T. Ly, N. Maxted, P.W. Cains, Organic Process Research and Development 9 (2005) 923–932.
- [9] D. Kashchiev, Nucleation: Basic Theory with Applications, Butterworth-Heinemann, Oxford, 2000.
- [10] O. Louisnard, F. Gomez, R. Grossier, Journal of Fluid Mechanics 577 (2007) 385–415.
- [11] O. Louisnard, F. Espitalier, in: 19th International Congress on Acoustics, Revista de Acustica, vol. 38, 3–4 [on CDROM, ISBN 84-87985-12-2], Madrid, Spain, 2007, pp. ULT-09-007, 1–6 (special issue).
- [12] B.D. Storey, A.J. Szeri, Proceedings of the Royal Society 456 (2000) 1685–1709.
- [13] R. Grossier, O. Louisnard, Y. Vargas, Ultrasonics Sonochemistry 14 (2007) 431–437.
- [14] D. Kashchiev, G.V. Rosmalen, Cryst. Res. Technol 38 (2003) 555–574.
- [15] R. Toegel, B. Gompf, R. Pecha, D. Lohse, Physical Review Letters 85 (15) (2000) 3165–3168.
- [16] S. Sawamura, T. Ishigami, N. Egoshi, M. Tsuchiya, Y. Taniguchi, K. Suzuki, High Pressure Research 11 (1994) 347–353.
- [17] M. Karapetianz, Thermodynamique chimique, mir 1978 Edition, MIR Moscou, Moscou, 1975.
- [18] Y. Hua, Z. Lin, Z. Yan, Minerals Engineering 15 (2002) 451–456.
- [19] D.W. Green, R.H. Perry, Perry's Chemical Engineers' Handbook, eighth ed., McGraw-Hill, 2008.
- [20] D.R. Lide, Handbook of Chemistry and Physics, 77th ed., CRC Press, 1996–1997.
- [21] W.F. Linke, Solubilities: Inorganic and Metal-organic Compounds. A Compilation of Solubility from the Periodical Literature, 4th ed., vol. II, American Chem. Soc., Washington, DC, 1965.
- [22] K. Ohsaka, E.H. Trinh, Applied Physics Letters 73 (1) (1998) 129–131.
- [23] D. Kashchiev, D. Verdoes, G.M. van Rosmalen, Journal of Crystal Growth 110 (1991) 373–380.
- [24] A. Mersmann, Crystallisation Technology Handbook, second ed., Marcel Dekker Inc., New York, 2001.
- [25] S. Hilgenfeldt, M.P. Brenner, S. Grossman, D. Lohse, Journal of Fluid Mechanics 365 (1998) 171–204.
- [26] O. Louisnard, F. Gomez, Phys. Rev. E 67 (3) (2003) 036610.
- [27] J. Miladinović, M. Todorović, R. Ninković, Chemical Thermodynamics 34 (2002) 1769–1776.
- [28] J.G. Albright, J.A. Rard, S. Serna, E. Summers, M.C. Yang, Chemical Thermodynamics 32 (2000) 1447–1487.
- [29] V. Gerbaud, N. Gabas, J. Blouin, C. Laguerie, Journal of Crystal Growth 166 (1996) 172–178.